# Robust super-twisting-based disturbance observer for autonomous underwater vehicles: Design, stability analysis, and real-time experiments

Jesus Guerrero, Ahmed Chemori, Vincent Creuze, Jorge Torres

# Highlights

## Robust super-twisting-based disturbance observer for autonomous underwater vehicles: design, stability analysis, and real-time experiments

Jesus Guerrero,Ahmed Chemori,Vincent Creuze,Jorge Torres

- A new disturbance observer based on the Super-Twisting Algorithm is proposed.
- A nominal PD is enhanced through the designed disturbance observer.
- The stability analysis of the overall closed-loop system is proved.
- The resulting robust PD is validated in real-time experiments on Leonard AUV.
- The real-time experiments demonstrate the effectiveness and robustness of the proposed scheme.

# Robust super-twisting-based disturbance observer for autonomous underwater vehicles: design, stability analysis, and real-time experiments

Jesus Guerrero[a], Ahmed Chemori[b,*], Vincent Creuze[b] and Jorge Torres[c]

[a]Tecnologico Nacional de MÃ!xico / ITS Abasolo, Guanajuato, Mexico
[b]LIRMM, University of Montpellier, CNRS, Montpellier, France
[c]Center for Research and Advanced Studies of the National Polytechnic Institute (CINVESTAV), Mexico city, Mexico

ARTICLE INFO

*Keywords*:
Sliding Mode Theory
Disturbance Observer
AUVs
Real-Time Experiments
Stability Analysis

ABSTRACT

This paper proposes a new observation-based proportional-derivative control method for robust trajectory tracking of autonomous underwater vehicles (AUVs). The proposed control scheme is designed based on a new observation-based nonlinear model that captures the dynamics and uncertainties of the AUV's behavior. The proposed control method is formulated in such a way that it can handle system nonlinearities and uncertainties, making it robust to external disturbances and model uncertainties. The effectiveness of the proposed control method is demonstrated through extensive real-time experiments in a real-world AUV trajectory tracking scenario. The obtained results show that the proposed control method outperforms other control methods in the literature regarding trajectory tracking accuracy, robustness, and disturbance rejection. Overall, the proposed observation-based proportional-derivative control method can significantly improve the trajectory tracking performance of AUVs in real-world applications.

## 1. Introduction and Related Work

Underwater vehicles have become increasingly important in various fields, such as ocean exploration, environmental monitoring, and underwater construction. However, the operation of these vehicles is often challenging due to significant disturbances such as ocean currents and waves, which can affect their stability and performance. To overcome these challenges, several control techniques have been proposed in the literature Tijjani, Chemori and Creuze (2022). For example, some of the most popular techniques used to control underwater vehicles thanks to their simplicity and good performance are the Proportional-Derivative (PD) and the Proportional-Integral-Derivative (PID) controllers and their nonlinear versions (see for instance, Herman (2009); Sarhadi, Noei and Khosravi (2016); Campos, Chemori, Creuze, Torres and Lozano (2017); Campos, Abundis, Chemori, Creuze and Torres (2019); Guerrero, Torres, Creuze, Chemori and Campos (2019c)). However, although PD control has the simplest control structure, it is well known that it shows steady-state error and is not robust towards external disturbances and parametric uncertainties. The performance of the PID may be degraded when dealing with highly nonlinear systems, time-varying disturbances, or with time delays. To address these limitations, nonlinear adaptations of PD/PID controllers have been designed, albeit at the cost of introducing more sophisticated techniques, potentially complicating the control scheme.

Besides, robust control methods have been developed to ensure accurate and reliable operation of underwater vehicles as an alternative solution for the AUV control problem. For instance, adaptive controllers Maalouf, Creuze and Chemori (2012), fuzzy controllers Xiang, Yu and Zhang (2017); Remmas, Chemori and Kruusmaa (2021), adaptive fuzzy sliding mode controllers Bessa, Dutra and Kreuzer (2008, 2010), neural network controllers Cui, Yang, Li and Sharma (2017), Backstepping technique An, Wang, He and Yuan (2022), Sliding Mode Controllers (SMC) Elmokadem, Zribi and Youcef-Toumi (2016); Guerrero, Chemori, Torres and Creuze (2023), adaptive SMC Guerrero, Torres, Creuze and Chemori (2019b); Qiao and Zhang (2019); Tijjani, Chemori and Creuze (2021).

Another effective method to control underwater vehicles is the disturbance observer based on the sliding mode technique. The sliding mode control method is well-known for its robustness and fast convergence in the presence of disturbances and uncertainties, making it a suitable choice for underwater vehicle control. The disturbance observer-based on the sliding mode technique, estimates and compensates for unknown disturbances by modifying the control input, improving the stability and performance of the control system. The disturbance observer based on SMC has been applied in several works such as in Chen (2003); Li, Yang, Chen and Chen (2011); Ginoya, Shendge and Phadke (2013); Wang, Meng and Huang (2017). In the paradigm of underwater vehicles, a disturbance observer based on the sliding mode technique was developed in Wang, Mihalec, Gong, Pompili and Yi (2018). The authors designed a disturbance observer based on the Super-twisting algorithm (STA)

*Corresponding author
jesus.gt@abasolo.tecnm.mx (J. Guerrero); ahmed.chemori@lirmm.fr (A. Chemori); vincent.creuze@lirmm.fr (V. Creuze); jtorres@ctrl.cinvestav.mx (J. Torres)
https://jnguerrero.github.io/ (J. Guerrero)
ORCID(s): 0000-0002-5873-8986 (J. Guerrero); 0000-0001-9739-9473 (A. Chemori)

for the trajectory tracking of an underwater vehicle. Then, the estimation of the disturbance made by the observer is introduced to a feedback linearization-based model predictive controller. Finally, the authors proved the effectiveness of the proposed controller through numerical simulations. However, although it presents interesting results, the authors proposed a disturbance observer and controller only consider the partial model of the underwater vehicle, controlling the $x$, $y$, and $\psi$ dynamics. Moreover, the observer and controller design needs the full knowledge of the dynamical system, which complicates its implementation in an actual underwater vehicle, because the hydrodynamic parameters change depending on the vehicle's operational condition.

In Guerrero, Torres, Creuze and Chemori (2019a), a disturbance observer has been developed based on the Generalized Super Twisting Algorithm (GSTA) to improve some non-robust controllers such as the non-linear PD control Campos et al. (2017) and the Backstepping method. Based on the obtained real-time experiments for the depth and yaw trajectory tracking, one can notice the effectiveness of the proposed methodology when dealing with parametric uncertainties and external disturbances. However, one drawback of this disturbance observer lies in a large number of observer gains to tune.

In the work of Nerkar, Londhe and Patre (2022), a disturbance observer based on the STA was designed for trajectory tracking of a linearized steering and the diving plane of an underwater vehicle. Through numerical simulations, the authors prove the effectiveness of the proposed scheme for trajectory tracking of an AUV in vertical and horizontal planes.

Finally, in Guerrero, Chemori, Torres and Creuze (2024), the authors developed a disturbance observer with adaptive laws for the tuning of the observer's gains. The algorithm was employed to improve the performance of the PD control through several real-time experiments.

Based on the cited literature, it is worth noting that the disturbance observers are designed to improve different kinds of controllers. In our approach, we decided to improve the well-known PD controller. Because this scheme is widely used when underwater vehicles are deployed at the sea. Generally, the ROV has an internal PD/PID controller to reach the desired position commanded by the user. Our philosophy is to maintain a simple structure for the controller while preserving the robustness toward parametric uncertainties and external disturbances. Moreover, this paper provides a comprehensive analysis of a disturbance observer based on the sliding mode technique for underwater vehicle control derived from Guerrero et al. (2019a). Indeed, the main idea is to simplify the design of the new disturbance observer inspired by the cited works about STA-based designs. The disturbance observer will be introduced in the nominal PD controller to provide robustness toward parametric uncertainties and external disturbances. The main contributions of this paper can be summarized as follows:

1. We develop a disturbance observer based on the technique of the extended state observer (ESO) and the STA. This observer will estimate the parametric uncertainties and external disturbances online, and this estimation will be inserted into a non-robust PD controller. The stability analysis of the resulting closed-loop, including both observer and controller, using the Lyapunov arguments, is provided.
2. Compared to the works of Wang et al. (2018); Guerrero et al. (2019a); Nerkar et al. (2022); Guerrero et al. (2024), the following features can be highlighted:
   (a) The proposed observer addresses the complete underwater vehicle nonlinear system.
   (b) The proposed disturbance observer does not need full knowledge of the hydrodynamics parameters.
   (c) We propose a simpler version compared to Guerrero et al. (2019a) without sacrificing the robustness of the proposed algorithm, with only two feedback gains to be tuned.
   (d) Compared to Guerrero et al. (2024), the proposed disturbance observer here is based on constant feedback gains. The proposed algorithm was able to improve the performance even of nonlinear controllers such as the Backstepping (BS) algorithm. Moreover, the non-adaptive STA observer is not a trivial case of the adaptive one. Indeed, the present contribution can be considered complementary to the work reported in Guerrero et al. (2024), where the advantages and complexities related to both the stability analysis and real-time applications are enlightened.
3. The effectiveness and robustness of the resulting robust PD controller (RPD) are demonstrated through several real-time experimental scenarios in different operating conditions. Compared to our previous work, we have added one more scenario in order to prove the robustness of the proposed methodology.

The rest of the paper is organized as follows: the mathematical modeling of underwater vehicles is given in Section 2. The design of the proposed robust disturbance observer based on the Super Twisting Algorithm is detailed in Section 3, while the stability analysis of the proposed observer is addressed in Section 4. In Section 5, the nominal PD controller, enhanced with the designed disturbance observer, is introduced, as well as its stability analysis. To demonstrate the effectiveness of the proposed methodology, several real-time experiments were carried out on a real platform and reported in Section 6. Finally, a conclusion and final remarks are drawn in Section 7.

## 2. Mathematical Model of the Underwater Vehicle

The mathematical model of underwater vehicles has been studied by several works such as Fossen (1999); Wadoo and Kachroo (2017); Sarhadi et al. (2016). The dynamic model in the body-fixed frame is given as follows:

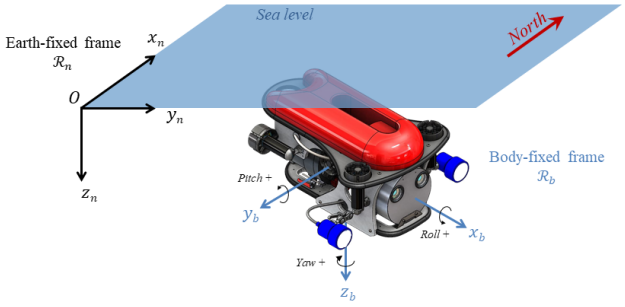


**Figure 1:** Illustration of the coordinate systems, including the earth-fixed frame $(x_n, y_n, z_n)$ and the body-fixed frame $(x_b, y_b, z_b)$.

$$M\dot{\nu} + C(\nu)\nu + D(\nu)\nu + g(\eta) = \tau + w_\nu(t) \tag{1}$$

The vector $\nu = [u, v, w, p, q, r]^T \in \mathbb{R}^6$ is the state vector of velocity relative to the body-fixed frame. The inertia matrix is denoted by $M \in \mathbb{R}^{6\times6}$, $C(\nu) \in \mathbb{R}^{6\times6}$ is the Coriolis-centripetal matrix, $D(\nu) \in \mathbb{R}^{6\times6}$ is the hydrodynamic damping matrix, $g(\cdot) \in \mathbb{R}^6$ is the vector of the gravitational and buoyancy forces and moments. Vector $\tau\ (\in \mathbb{R}^6)$ is the control input acting on the vehicle and $w_\nu(t) \in \mathbb{R}^6$ is the vector of the external disturbances effects.

The dynamics of the underwater vehicle can be expressed in the earth-fixed frame (as illustrated in Fig. 1) using the matrix transformation $J(\eta) \in \mathbb{R}^{6\times6}$ defined as:

$$\dot{\eta} = J(\eta)\nu \tag{2}$$

where $\eta = [x, y, z, \phi, \theta, \psi]^T$ is the vector of position and orientation of the vehicle in the earth-fixed frame; while, $\dot{\eta}$ denotes the time derivative of the vector $\eta$. Applying (2) to (1) yields to the following representation in the earth-fixed frame:

$$M_\eta(\eta)\ddot{\eta} + C_\eta(\nu,\eta)\dot{\eta} + D_\eta(\nu,\eta)\dot{\eta} + g_\eta(\eta) = \tau_\eta(\eta) + \overline{w}_\eta(t) \tag{3}$$

where:

$$\begin{aligned}
M_\eta(\eta) &= J^{-T}(\eta) M J^{-1}(\eta) \\
C_\eta(\nu,\eta) &= J^{-T}(\eta)\left[C(\nu) - M J^{-1}(\eta)\dot{J}(\eta)\right] J^{-1}(\eta) \\
D_\eta(\nu,\eta) &= J^{-T}(\eta) D(\nu) J^{-1}(\eta) \\
g_\eta(\eta) &= J^{-T}(\eta) g(\eta) \\
\tau_\eta(\eta) &= J^{-T}(\eta)\tau \\
\overline{w}_\eta(t) &= J^{-T}(\eta) w_\nu(t)
\end{aligned} \tag{4}$$

It is well known that model-based controllers require the full knowledge of the dynamical model. However, in underwater robotics, it is not easy to estimate the hydrodynamic parameters because their values may depend on the operating conditions, the salinity of the water, etc. For the above mentioned reasons, we express the dynamics of the vehicle shown in (3) in terms of the nominal parameters as follows:

$$\hat{M}_\eta(\eta)\ddot{\eta} + \hat{C}_\eta(\nu,\eta)\dot{\eta} + \hat{D}_\eta(\nu,\eta)\dot{\eta} + \hat{g}_\eta(\eta) = \tau_\eta(\eta) + w_\eta(t) \tag{5}$$

where $\hat{M}_\eta$, $\hat{C}_\eta$, $\hat{D}_\eta$, $\hat{g}_\eta$ represent the estimation of the matrices of the dynamical model. The vector $w_\eta(t)$ is defined as:

$$w_\eta(t) = \overline{w}_\eta - \tilde{f}(\cdot) \tag{6}$$

It is worth noting that the vector $w_\eta(t)$ includes the external disturbances and the unknown dynamics of the model denoted by $\tilde{f}(\cdot)$ and is defined as:

$$\tilde{f}(\cdot) = (M_\eta - \hat{M}_\eta)\ddot{\eta} + (C - \hat{C}_\eta)\dot{\eta} + (D - \hat{D}_\eta)\dot{\eta} + (g_\eta - \hat{g}_\eta) \tag{7}$$

Note that the dynamics are rewritten in terms of the known hydrodynamic parameters $\hat{f}(\cdot)$ and the lumped vector $w_\eta(t)$ including the unknown dynamics and the bounded external disturbances.

## 3. Proposed STA-Based Disturbance Observer Design

In this section, a robust STA-Based disturbance observer is designed. The proposed methodology is based on the Extended State Observer methodology (ESO) Han (1995). In brief, the ESO technique is applied to a chain systems form, where the external disturbance is seen as an augmented state. Then, the ESO will estimate both the state variables and the external disturbances Han (2009).

To give a comprehensive and detailed explanation of the disturbance observer, let us rewrite the dynamical model (5) in integrator form, by selecting the following state variables:

$$z_1 = \eta \quad ; \quad z_2 = \dot{\eta}$$

Then, the dynamical model (5) can be expressed as follows:

$$\begin{aligned}
\dot{z}_1 &= z_2 \\
\dot{z}_2 &= \hat{F}(z) + \hat{G}(z)u(t) + d(t)
\end{aligned} \tag{8}$$

where:

$$\begin{aligned}
\hat{F}(z) &= -\hat{M}_\eta(\eta)^{-1}\left[\hat{C}_\eta(\nu,\eta)\dot{\eta} + \hat{D}_\eta(\nu,\eta)\dot{\eta} + \hat{g}_\eta(\eta)\right] \\
\hat{G}(z) &= \hat{M}_n(\eta)^{-1} J^{-T}(\eta) \\
d(t) &= \hat{M}_\eta(\eta)^{-1} w_\eta(t) \\
u(t) &= \tau_\eta
\end{aligned}$$

Finally, classical assumptions in underwater vehicles can be pointed out:

**Assumption 1**. The pitch angle is smaller than $\pi/2$, i.e., $|\theta| < \pi/2$.

**Assumption 2**. The time-derivative of the perturbation $d(t)$ is bounded.

Assumption 1 ensures that the inverse of the matrix $J(\eta)$ always exists; consequently, the term $G(z)$ exists. In a physical scenario, a pitch close to $\pi/2$ implies that the robot dives vertically, which is generally not required during sea missions.

Assumption 2 ensures that the disturbance, and especially its time-derivative is bounded as follows:

$$|\dot{d}_i(t,x)| \leq \delta_i \tag{9}$$

where $\delta_i \geq 0$ for $i = \overline{1,6}$.

Considering the following auxiliary variable defined:

$$\sigma(t) = z_2 + \Gamma z_1 \tag{10}$$

where $\sigma \in \mathbb{R}^6$ and $\Gamma = diag\{\gamma_1, \gamma_2, \cdots, \gamma_6\}$ is a diagonal positive definite matrix.

The time derivative of $\sigma(t)$ is computed as follows:

$$\dot{\sigma}(t) = f(z) + g(z)u(t) + d(t) \tag{11}$$

where $f(z) = \hat{F}(z) + \Gamma\dot{z}_1$, and $g(z) = \hat{G}(z)$

From the dynamics of the auxiliary variable (11), the lumped disturbance will be considered as an extended state $h(t)$, such that:

$$\begin{aligned} \dot{\sigma}(t) &= f(z) + g(z)\tau_\eta + h(t) \\ \dot{h}(t) &= \xi(t) \end{aligned} \tag{12}$$

where $\xi(t)$ is the time derivative of the total disturbance $d(t)$.

The proposed disturbance observer dynamics for the system (12) can be defined as:

$$\begin{aligned} \dot{\hat{\sigma}} &= f(z) + g(z)\tau_\eta - K_1\Phi_1(\tilde{\sigma}) + \hat{d}(t) \\ \dot{\hat{d}} &= -K_2\Phi_2(\tilde{\sigma}) \end{aligned} \tag{13}$$

where $K_1 = diag\{k_{11}, k_{12}, \cdots, k_{16}\}$ and $K_2 = diag\{k_{21}, k_{22}, \cdots, k_{26}\}$ are diagonal positive definite matrices representing the observer feedback gain. The vectors $\Phi_1$ and $\Phi_2$ are defined as $\Phi_1(\tilde{\sigma}) = [\phi_{11}, \phi_{12}, \cdots, \phi_{16}]]^T$ and $\Phi_2(\tilde{\sigma}) = [\phi_{21}, \phi_{22}, \cdots, \phi_{26}]^T$, and each element of these vectors is given by:

$$\begin{aligned} \phi_{1i}(\tilde{\sigma}_i) &= |\tilde{\sigma}_i|^{1/2}\text{sgn}(\tilde{\sigma}_i) \\ \phi_{2i}(\tilde{\sigma}_i) &= \frac{1}{2}\text{sgn}(\tilde{\sigma}_i) \end{aligned} \tag{14}$$

Finally, the estimation errors are deduced as:

$$\tilde{\sigma}(t) = \hat{\sigma}(t) - \sigma(t) \tag{15}$$

$$\tilde{d}(t) = \hat{d}(t) - d(t) \tag{16}$$

where $\hat{\sigma}(t)$ and $\hat{d}(t)$ are the estimated observer internal states. $\dot{\hat{\sigma}}(t)$ and $\dot{\hat{d}}(t)$ are the dynamics of the estimated observer internal states.

## 4. Disturbance observer stability analysis

This section presents the stability analysis of the disturbance observer based on the STA algorithm (13)-(14). The STA algorithm has two main characteristics: finite-time stability and robustness against matched disturbances Moreno (2009). For completeness, we recall the concept of stability in finite time for a system $\dot{x} = f(t,x)$ with initial condition $x(t_0) = x_0$, where the solution of the system is denoted by $x(t,x_0)$ for a given initial condition $x_0$ belonging to a compact subspace $\mathcal{D} \subset R^n$. It is assumed that $x = 0$ is an equilibrium point of the system, see Orlov (2004).

**Definition 1.** *The equilibrium point $x = 0$ of the system $\dot{x} = f(t,x)$ is said to be stable in finite time if it is asymptotically stable and any solution $x(t,x_0)$ of the system achieves equilibrium at some moment of finite time, i.e.*

$$x(t,x_0) = 0 \quad \textit{for all} \quad t \geq T(x_0)$$

*where $T : R^n \to R_+ \cup \{0\}$ is the so-called stabilization time function.*

In the following theorem, we establish the stability of the disturbance observer.

**Theorem 2.** *Consider the augmented system dynamics (12). The Super Twisting-based Algorithm (13) is a finite-time stable disturbance observer provided that $K_1, K_2$ are positive definite matrices.*

Proof. First of all, let us compute the time derivative of the estimation errors (15) and (16), and this yields:

$$\begin{aligned} \dot{\tilde{\sigma}} &= -K_1|\tilde{\sigma}|^{1/2}\text{sgn}(\tilde{\sigma}) + \tilde{d} \\ \dot{\tilde{d}} &= -K_2\text{sgn}(\tilde{\sigma}) - h(t) \end{aligned} \tag{17}$$

To give a more comprehensive explanation of the stability of the proposed observer, let us consider the following change of variables:

$$\begin{aligned} s_{1i} &= \tilde{\sigma}_i \\ s_{2i} &= \tilde{d} = -k_{2i}\int_0^t \text{sgn}(\tilde{\sigma}(\tau) + h(\tau))d\tau \end{aligned}$$

Then (17) can be rewritten in a scalar form for ($i = \overline{1,6}$) as follows:

$$\begin{aligned} \dot{s}_{1i} &= -k_{1i}|s_{1i}|^{\frac{1}{2}}\text{sgn}(s_{1i}) + s_{2i} \\ \dot{s}_{2i} &= -k_{2i}\text{sgn}(s_{1i}) + h_i(t) \end{aligned} \tag{18}$$

Without loss of generality, we can rewrite (18) with simplified notations as follows:

$$\begin{aligned} \dot{s}_1 &= -k_1|s_1|^{\frac{1}{2}}\text{sgn}(s_1) + s_2 \\ \dot{s}_2 &= -k_2\text{sgn}(s_1) + h(t) \end{aligned} \tag{19}$$

Note that if we select the state vector $\zeta = [\zeta_1, \zeta_2]^T = [|s_1|^{\frac{1}{2}}\text{sgn}(s_1), s_2]^T$, then we can rewrite the dynamics (19) as follows:

$$\dot{\zeta} = \frac{1}{|\zeta_1|}\Big[A\zeta + B\rho\Big] \tag{20}$$

with:

$$A = \begin{bmatrix} -\frac{1}{2}k_1 & \frac{1}{2} \\ -k_2 & 0 \end{bmatrix}; \qquad B = \begin{bmatrix} 0 \\ 1 \end{bmatrix} \tag{21}$$

and $\rho = |\zeta_1|h(t)$, which satisfies $|\rho| \leq \delta|\zeta_1|$. Moreover, the transformed perturbation satisfies the sector condition as stated in Moreno (2009). This means that, $\omega(\rho, \zeta) = -\rho^2(t, \zeta) + \delta^2\zeta_1^2 \geq 0$.

To prove the stability of the equilibrium point $(s_1, s_2) = (0, 0)$, let us consider the strong Lyapunov function Moreno and Osorio (2008):

$$V = \zeta^T P \zeta \tag{22}$$

where $P$ is a positive definite matrix that satisfies the Lyapunov equation:

Now, by selecting positive feedback gains, we can ensure that the Lyapunov function is positive definite and radially unbounded; this means that:

$$\lambda_{\min}\{P\}\|\zeta\|_2^2 \leq V(s) \leq \lambda_{\max}\{P\}\|\zeta\|_2^2 \tag{23}$$

where $\lambda_{\min}$ and $\lambda_{\max}$ is the smallest and greatest eigenvalue of $P$, respectively. $\|\zeta\|_2^2 = |s_1| + s_2^2$ is the Euclidean norm of $\zeta$.

Taking the time derivative of $V$ along the trajectories of the system yields:

$$\begin{aligned}
\dot{V} = & \quad \tfrac{1}{|\zeta_1|}\begin{bmatrix}\zeta \\ \rho\end{bmatrix}^T \begin{bmatrix} A^TP + PA & PB \\ B^TP & 0 \end{bmatrix}\begin{bmatrix}\zeta \\ \rho\end{bmatrix} \\
\leq & \quad \tfrac{1}{|\zeta_1|}\left\{\begin{bmatrix}\zeta \\ \rho\end{bmatrix}^T \begin{bmatrix} A^TP + PA & PB \\ B^TP & 0 \end{bmatrix}\begin{bmatrix}\zeta \\ \rho\end{bmatrix} + \omega(\rho, \zeta)\right\} \\
= & \quad \tfrac{1}{|\zeta_1|}\left\{\begin{bmatrix}\zeta \\ \rho\end{bmatrix}^T \begin{bmatrix} A^TP + PA + \delta^2C^TC & PB \\ B^TP & -1 \end{bmatrix}\begin{bmatrix}\zeta \\ \rho\end{bmatrix}\right\} \\
= & \quad \tfrac{1}{|\zeta_1|}\begin{bmatrix}\zeta \\ \rho\end{bmatrix}^T \underbrace{\begin{bmatrix} A^TP + PA + \delta^2C^TC + \overline{\alpha}P & PB \\ B^TP & -1 \end{bmatrix}}_{W(\cdot)}\begin{bmatrix}\zeta \\ \rho\end{bmatrix} \\
& \quad -\tfrac{\overline{\alpha}}{|\zeta_1|}\zeta^T P\zeta
\end{aligned}$$

From the above $C = [1\ 0]$. If we select the feedback gains $k_1, k_2$ positive, the system $(A, B, C)$ is controllable and observable. Then, using the bounded-real lemma Boyd, El Ghaoui, Feron and Balakrishnan (1994), we can ensure that the LMI is feasible if the system is non-expansive. As a consequence, it is always possible to ensure that $W(\cdot) \leq 0$.

$$\dot{V} \leq -\frac{\overline{\alpha}}{|\zeta_1|}\zeta^T P\zeta = -\frac{\overline{\alpha}}{|\zeta_1|}V(\zeta) \tag{24}$$

Then, it is possible to express (23) as follows:

$$|\zeta_1| \leq \|\zeta\|_2 \leq \frac{V^{\frac{1}{2}}(\zeta)}{\lambda_{\min}^{\frac{1}{2}}\{P\}} \tag{25}$$

Substituting this in $\dot{V}$, leads to:

$$\dot{V} \leq -\overline{\alpha}\lambda_{\min}^{\frac{1}{2}}\{P\}V^{1/2}(\zeta) \tag{26}$$

The differential inequality guarantees the finite time convergence of the equilibrium point to zero, Moreno and Osorio (2008). This means that, by the comparison principle, the observer internal states $(\hat{\sigma}, \hat{d})$ converge to $(\sigma, d)$ at latest after a time given by:

$$T = \frac{2V^{\frac{1}{2}}(0)}{\overline{\alpha}\lambda_{\min}^{\frac{1}{2}}\{P\}} \tag{27}$$

which ends the proof.

## 5. Enhancing non-robust controllers

The PD control is a well-known simple controller used in the paradigm of AUVs. For instance, in the work Campos et al. (2017), the authors have developed a non-linear PD (NLPD) controller for trajectory tracking. The authors compare the proposed NLPD with the nominal PD design in this work. The results section shows that both controllers perform well when the nominal case is considered. However, when the hydrodynamics parameters of the vehicle change, the controller's performance is severally degraded, even for the NLPD. Taking this issue as a primary motivation, we propose a new enhanced PD control based on the ESO technique with the designed disturbance observer.

The PD nominal design is borrowed from Campos et al. (2017) and is given by:

$$\tau_{nom} = \hat{M}_\eta\ddot{\eta}_d + \hat{C}_\eta\dot{\eta}_d + \hat{D}_\eta\dot{\eta}_d + g_\eta(\eta) - K_p e(t) - K_d\dot{e}(t) \tag{28}$$

where the trajectory tracking error is defined as $e(t) = [e_1(t), \cdots, e_6(t)] = \eta - \eta_d$ and the desired trajectory $\eta_d = [x_d(t), y_d(t), z_d(t), \phi_d(t), \theta_d(t), \psi_d(t)]^T$. In turn, $K_p, K_d \in \mathbb{R}^{6\times6}$ are diagonal positive definite matrices representing the controller feedback gains.

### 5.1. Improved PD controller design

In order to improve the performance of the nominal PD design, we propose to incorporate the estimated disturbance to counteract its adverse effect. Then the following Robust PD (RPD) controller is proposed:

$$\tau_\eta(\eta) = \tau_{nom} - \hat{M}_\eta\hat{d} - \hat{K}\text{SGN}(\dot{e}) \tag{29}$$

where $\hat{d}(t)$ is the estimation of the disturbances provided by the observer dynamics (13). The vector $\text{SGN}(\dot{e}) =$

$[\text{sgn}(\dot{e}_1(t)), \text{sgn}(\dot{e}_2(t)), \cdots, \text{sgn}(\dot{e}_6(t))]$ and $\hat{K}$ is an adaptive gain, computed from the following dynamic equation:

$$\dot{\hat{K}} = \beta \|\dot{e}\| \tag{30}$$

where $\beta \in \mathbb{R}$ is a positive constant.

Finally, the closed-loop dynamics stability analysis is given in the next section.

**Remark 1.** The PD controller enhanced with the STA-based disturbance observer is described in Eq. (29). One can notice that the controller has three main terms. The first term is the nominal PD given in (28). The second term is related to the disturbance estimation made by the STA-based disturbance observer. The third term $\hat{K}SGN(\dot{e})$ is an adaptive term that is related to (40). In practical applications, the term $\beta$ is set to a small value near zero. Indeed, during our real-time experiments, the described term had a value of almost zero.

**Remark 2.** It is worth emphasizing that the proposed STA-based enhanced PD controller is endowed with two important features, including (i) it enables the estimation of the external disturbance, and (ii) it allows also the attenuation of the measurement noise, often present in most of the used sensors in robotics.

### 5.2. Closed-loop stability analysis

Given the underwater vehicle dynamics (5), by injecting the control law (29), we obtain the following closed-loop system:

$$\frac{d}{dt}\begin{bmatrix} e \\ \dot{e} \end{bmatrix} = \begin{bmatrix} \dot{e} \\ -M_\eta(\eta)^{-1}\Big[[\hat{C}_\eta(\nu,\eta) + \hat{D}_\eta(\nu,\eta) + K_d]\dot{e} + K_p e \\ +\hat{K}\text{SGN}(\dot{e})\Big] - \hat{d}(t) + d(t) \end{bmatrix} \tag{31}$$

Consider the following candidate Lyapunov function:

$$V(e,\dot{e}) = \frac{1}{2}\dot{e}^T \hat{M}_\eta(\eta)\dot{e} + \frac{1}{2}e^T K_p e + \frac{1}{2\beta}\tilde{K}^2 \tag{32}$$

where $K_p$ is a diagonal definite positive matrix, $\beta$ is a positive constant, introduced in (40), and $\tilde{K} = \hat{K} - K$ is the parameter estimation error.

Now, taking the time derivative of $V$ yields:

$$\dot{V}(e,\dot{e}) = \dot{e}^T \hat{M}_\eta(\eta)\ddot{e} + \frac{1}{2}\dot{e}^T \dot{\hat{M}}_\eta(\eta)\dot{e} + e^T K_p \dot{e} + \frac{1}{\beta}\tilde{K}\dot{\hat{K}} \tag{33}$$

Substituting the error dynamics (31) into the time derivative of $V$, leads to:

$$\begin{aligned} \dot{V}(e,\dot{e}) \quad &= \tfrac{1}{2}\dot{e}^T\Big[\dot{\hat{M}}_\eta(\eta) - 2\hat{C}_\eta(\nu,\eta)\Big]\dot{e} - \dot{e}^T\Big[\hat{D}_\eta(\nu,\eta) + K_d\Big]\dot{e} \\ &\quad + \dot{e}^T[d(t) - \hat{d}(t)] - \hat{K}\dot{e}^T\text{SGN}(\dot{e}) + \tfrac{1}{\beta}\tilde{K}\dot{\hat{K}} \end{aligned} \tag{34}$$

Recalling that, within the Lagragian approach, $[\dot{\hat{M}}_\eta(\eta) - 2\hat{C}_\eta(\nu,\eta)]$ is a skew-symmetric matrix, Fossen (1999); then, we obtain:

$$\begin{aligned} \dot{V}(e,\dot{e}) &= -\dot{e}^T\Big[\hat{D}_\eta(\nu,\eta) + K_d\Big]\dot{e} + \dot{e}^T[d(t) - \hat{d}(t)] \\ &\quad - \hat{K}\dot{e}^T\text{SGN}(\dot{e}) + \frac{1}{\beta}\tilde{K}\dot{\hat{K}} \\ &= -\dot{e}^T\Big[\hat{D}_\eta(\nu,\eta) + K_d\Big]\dot{e} + \dot{e}^T[d(t) - \hat{d}(t)] \\ &\quad - \hat{K}\sum_{i=0}^{6}|\dot{e}_i| + \frac{1}{\beta}\tilde{K}\dot{\hat{K}} \\ &\leq -\lambda_{\min}\{\hat{D}_\eta(\nu,\eta) + K_d\}\|\dot{e}\|^2 + K\|\dot{e}\| \\ &\quad - \hat{K}\|\dot{e}\| + \tilde{K}\|\dot{e}\| \\ &= -\lambda_{\min}\{\hat{D}_\eta(\nu,\eta) + K_d\}\|\dot{e}\|^2 \end{aligned} \tag{35}$$

We can notice that the matrix $K_d$ was selected positive definite in the controller design and the damping matrix is $\hat{D}_\eta > 0$ (see Fossen (1999)). This means that the function $\dot{V}$ is negative semi-definite. However, by applying Krasovskii-Lasalle's invariance principle, we can conclude that the equilibrium point is asymptotically stable.

## 6. Real-time experimental results

In order to demonstrate the practical viability of the proposed controller that was developed, it was implemented on the *Leonard* Tijjani, Chemori, Ali and Creuze (2023), an Unmanned Underwater Vehicle (UUV) designed at LIRMM laboratory (University of Montpellier, France). This underwater robot is a tethered vehicle, measuring 75 x 55 x 45 cm in size and weighing 28 kg. It is powered by six thrusters, which make it a holonomic fully actuated vehicle.

The test-bed of the robot comprises an UUV controlled by a laptop computer featuring an Intel Core i7-3520M 2.9 GHz CPU and 8 GB RAM. The computer operates under Windows 10 OS, and the control software is coded using Visual C++ 2015. The laptop collects data from the ROV's pressure and attitude (IMU) sensors, computes the control algorithms, and transmits commands to 6 *Syren10* Motor Drive that regulate the ROV's actuators. Table 1 provides a summary of the primary features of the vehicle.

To validate the efficacy and robustness of the proposed control algorithm, several experimental tests were conducted in the engineering pool at LIRMM, depicted in Figure 2. The basin measures 4 × 3 × 2 m and has a capacity of approximately 12 000 liters as illustrated in Figure 2. Although the control laws developed are intended for the full six-degrees-of-freedom system, the real-time experiments presented in this paper concentrate on depth and yaw dynamics. The primary goal of the proposed control law is to robustly track a predefined trajectory for depth and yaw despite the presence of external disturbances and/or parametric uncertainties. However, it is considered, thanks to the design of the vehicle, that the orientation angles $\phi$ and $\theta$ are naturally stable. Concerning the positioning of the vehicle, the X-Y measurements are not available because our underwater

**Table 1**
Main Features of the underwater vehicle

| | |
|---|---|
| Mass | 28 $kg$ |
| Buoyancy | 9 $N$ |
| Dimensions | $75 \times 55 \times 45$ cm |
| Maximal depth | 100m |
| Thrusters | 6 Seabotix BTD150 |
| Power | 24V - 600 W |
| Attitude Sensor | Invensense MPU-6000 MEMS 3-axis gyro and accelerometer<br>3-axis I2C magnetometer HMC-5883L<br>Atmega328 microprocessor |
| Camera | Pacific Co. VPC-895A<br>CCD1/3 PAL-25-fps |
| Depth sensor | Pressure Sensor MS5803-02BA |
| Sampling period | 50 ms |
| Surface computer | Dell Latitude E6230- Intel Core i7 -2.9 GHz<br>Windows 10 Professional 64 bits<br>Microsoft Visual C++ 2015 |
| Tether length | 30 m |

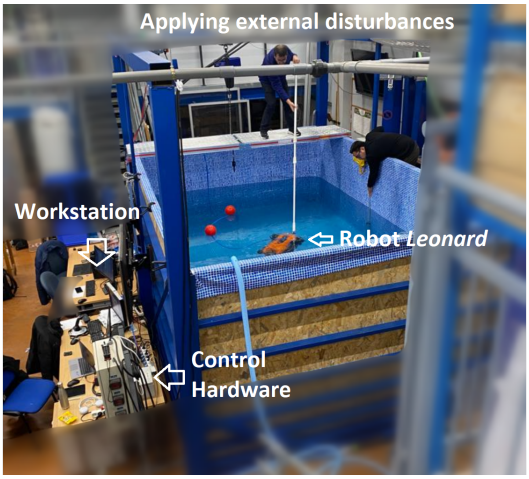


**Figure 2:** View of the test-bed for the real-time experiments. In the figure, one can note the Leonard robot and the workstation setup.

vehicle lacks a DVL or a camera to estimate them. Table 1 summarizes the control gains applied the real-time experiments. The proposed controllers were implemented on the *Leonard* underwater vehicle for the experimental investigations presented in this paper.

### 6.1. Real-Time Experimental Scenarios

In order to validate the robustness of the proposed controller, we test robust PD in different scenarios, including:

1. *Nominal Scenario:* This test is considered the case without external disturbances, and the robot will track a trajectory in depth and yaw at the same time.
2. *Parametric uncertainties scenario:* In this test, we modify the underwater vehicle's hydrodynamic parameters to test the proposed controller's robustness. To this end, we attach a floater to the vehicle's body to modify the robot's buoyancy. To change the damping of the robot, we have attached a rigid plastic sheet of dimension 45 $cm \times 20$ $cm$. Both, the floater and the plastic sheet can be seen in Figure 3.
3. *Robustness towards sudden mass variation:* In this scenario, we try to recreate the robot carrying an object for a while and release it. For this purpose, we attached a 60-cm long rope to the body of the robot with a 335 grams mass at the end of the rope, as illustrated in Figure 4.
4. *Robustness towards external disturbances:* In this case, we apply disturbances to the robot when the robot is tracking the trajectory. In this scenario, we push the robot with a stick several times, as shown in Fig. 5.

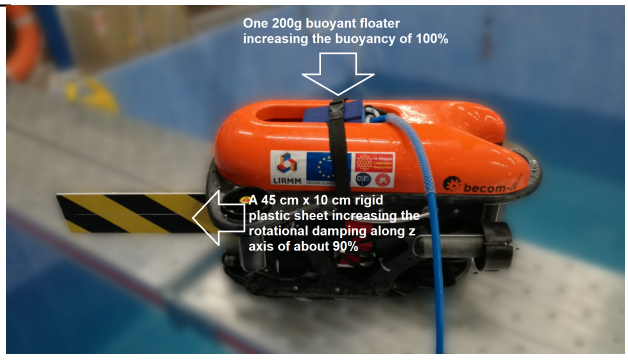


**Figure 3:** Configuration for the scenario 2. We add a 200g floater to increase the buoyancy up to 100%. A rigid plastic sheet of dimensions 45 $cm \times 10$ $cm$ is also added to the robot's body to increase the rotational damping along the z-axis of about 90%.

### 6.2. Performance Criteria

To fairly compare the performance of reference trajectory tracking for each controller, we use the following criteria:

- The Root Mean Square Error (RMSE) is defined as follows:

$$RMSE = \sqrt{\frac{1}{T_f}\int_0^{T_f} \|e(t)\|^2 dt} \tag{36}$$

  where $T_f$ denotes the duration of the experimental test, and $e(t)$ is the tracking error.

- To evaluate the energy consumption, we propose to use the integral of the control input index (INT), which is defined as follows:

$$INT = \int_{t_i}^{t_f} |\tau(t)| dt \tag{37}$$


**Figure 4:** Configuration for the scenario 3. A 335 gr weight is attached to the body of the vehicle to introduce a sudden mass change when the robot tracks a time-varying trajectory in depth (when the weight touches the bottom, then it is like its mass becomes null).

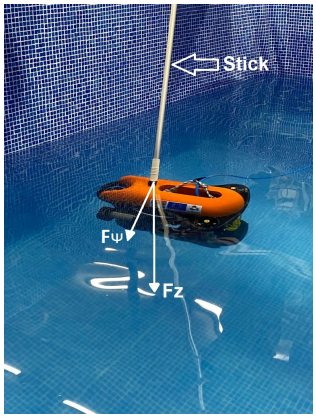


**Figure 5:** External disturbances applied to the underwater vehicle for scenario 4. During the experiment, we applied to push forces to disturb the depth and yaw dynamics simultaneously.

where $\tau(t)$ is the vector of position/attitude control input. The terms $t_i$ and $t_f$ denote the initial and final time of the experiment, respectively.

#### 6.2.1. Nominal Case

The trajectory tracking on depth and yaw for the nominal case is depicted at the top of Figure 6. From this figure, we can observe that both the PD and RPD controllers perform well. However, it can be seen that the RPD's behavior has better tracking errors than the nominal PD. The better performance of the proposed controller can also be numerically quantified by the Root Mean Square Error (RMSE), as seen in Table 2. The tracking errors for this scenario are depicted in the middle of Figure 6. From this graph, we can observe that the RPD performs better than the PD. Finally, at the bottom of this figure, we plotted the force and torque generated by the controllers for this experiment. As expected, the RPD demands slightly more energy than the nominal PD.

The RMSE criteria for the nominal case are summarized in the first row of Table 2. As we can see, the RPD controller performs better in trajectory tracking of the depth. However, the PD performs slightly better than the RPD when the yaw tracking is evaluated.

The energy consumption for this scenario is summarized in the first row of Table 3. It is possible to observe that the RPD requires more energy to reduce the trajectory tracking errors compared to the nominal PD.

Finally, the estimated disturbance for the nominal case is displayed in the first row of Figure 10.

#### 6.2.2. Robustness towards parametric uncertainties

As stated above, to modify the hydrodynamic parameters of the vehicle, we have attached a floater and a rigid plastic sheet with dimensions of 45 $cm \times 10$ $cm$ to increase the floatability up to 100% and the damping of the vehicle up to 90%.

At the top of Figure 7, we observe the trajectory tracking for the depth and yaw. As we can see, the nominal PD (blue line) is not able to reject the added parametric uncertainties, and the tracking error is constant during the whole test. However, the proposed robust controller (red line) manages the added disturbances and tracks the reference trajectory with smaller errors. The same happens when we analyze the trajectory tracking of the yaw, and it is also possible to observe a better performance of the proposed RPD over the nominal design. We can observe the evolution versus time of the trajectory tracking errors in the middle of the figure. At the bottom of the figure, the evolution of the control inputs is shown. One can note that the RPD requires slightly more energy to counteract the effect of the disturbance, as may be expected.

The RMSE criteria for this scenario are summarized in the second row of Table 2. As we can see, the RPD controller performs better in both tracking trajectory tasks.

From the energy consumption point of view, the RPD requires slightly more energy to compensate for the parametric uncertainties. However, based on the obtained results of the integral of the control input summarized in the second row of Table 3, we can observe that the PD requires more energy to try to reduce the steady-state error, this could be explained because the controller gains were low.

Finally, the estimated disturbances in the current robustness scenario is depicted in the second row of Figure 10.

#### 6.2.3. Robustness towards sudden mass variation

The results for trajectory tracking, in the depth and yaw, are depicted at the top of Figure 8. It is possible to observe that the weight touches the floor 25 seconds after the test has started. One can notice that the proposed RPD can handle this sudden change without any problem. Then, the robot moves towards the surface and carries the weight, then at the time of 40 seconds, the weight is no longer in contact with the ground, producing a persistent disturbance

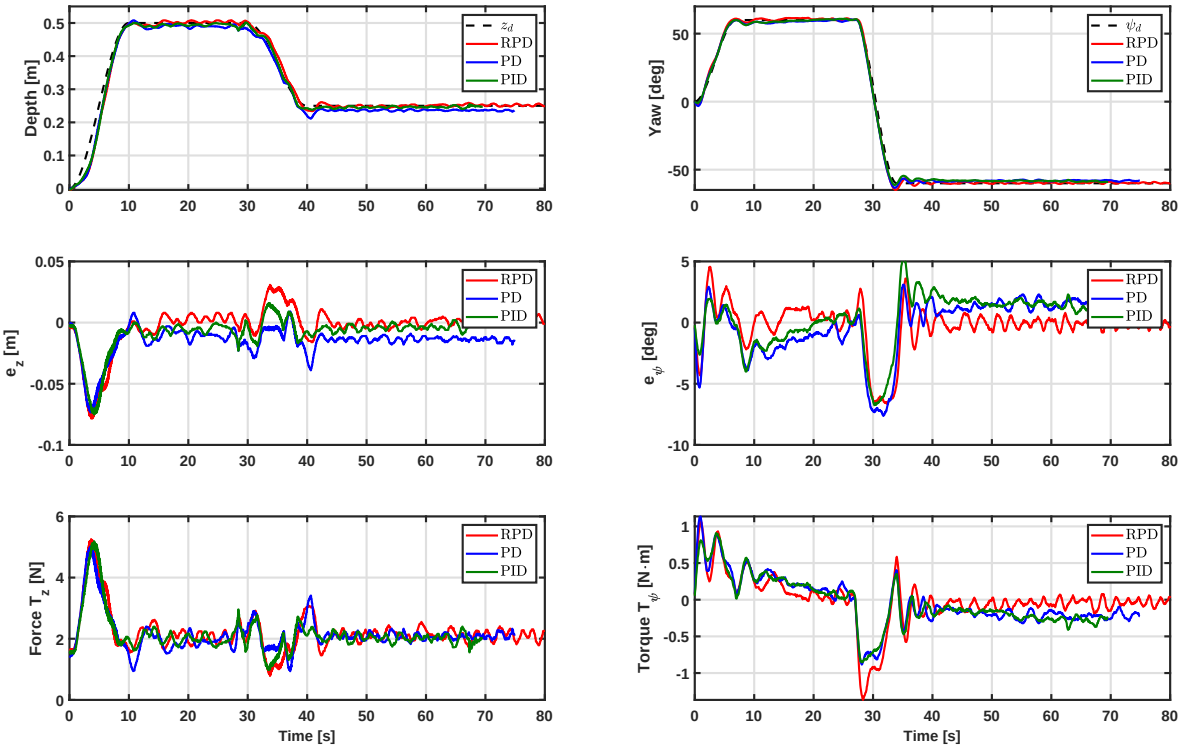


**Figure 6:** Scenario 1- Nominal Case. Experimental results of the trajectory tracking in depth and yaw, the desired trajectory is represented by the black dashed line, the PD with a solid blue line, the PID with a solid green line, and the proposed RPD controller with a solid red line.

due to the extra mass added to the robot. From this test, we can observe that both controllers have a good tracking performance. However, at the end of the test, it is possible to observe that the RPD reduces the tracking error. In the middle of the figure, we can see the plots of the evolution of the tracking errors. Note that the depth tracking error goes to zero, while the yaw error remains near to zero for the RPD; however, the PD shows a steady state error of almost 2 degrees. Finally, at the bottom of the figure, the forces and torques generated by the controllers are shown. Again, the control effort of the RPD is higher than the PD because of its disturbance rejection feature.

The RMSE values for this scenario are summarized in the third row of Table 2. From the presented data, we can conclude that the proposed RPD outperforms the PD nominal design.

In this case, the RPD requires slightly more energy to compensate for the extra weight attached to the robot, as we can see in the third row of Table 3.

Finally, the estimated disturbances, in the case of an aggregated external mass, are depicted in the third row of Figure 10.

#### *6.2.4. External disturbance rejection scenario*

In this scenario, the robot will perform the same tracking control goal as in the nominal case without considering any parametric uncertainty. However, to test the robustness of the proposed controller, we have applied several disturbances to the robot body with a long stick, as illustrated in Figure 5.

The results of this scenario are depicted in Figure 9. At the top of the figure, we can observe the effects of the disturbance on both, depth, and yaw. We have applied six disturbances throughout the experiment, and we can note that the robot is able to recover from each disturbance effect, as seen at the top of Figure 9. Besides, it is worth highlighting that some of the applied disturbances at the end of the experiment were conducted to disturb both dynamics simultaneously, and the controller was capable of managing both disturbances as well. The tracking errors are plotted in the middle of the figure, and we can note the impact of the applied disturbances. Finally, at the end of the figure, the evolution of the control inputs (force and torque) given by the controller is depicted.

The RMSE criterion of this experiment, for the proposed controller, is summarized in the fourth row of Table 2. In this stage, we do not compare this controller with the PD nominal design because all the disturbances were applied by human intervention and it is not possible to reproduce exactly the

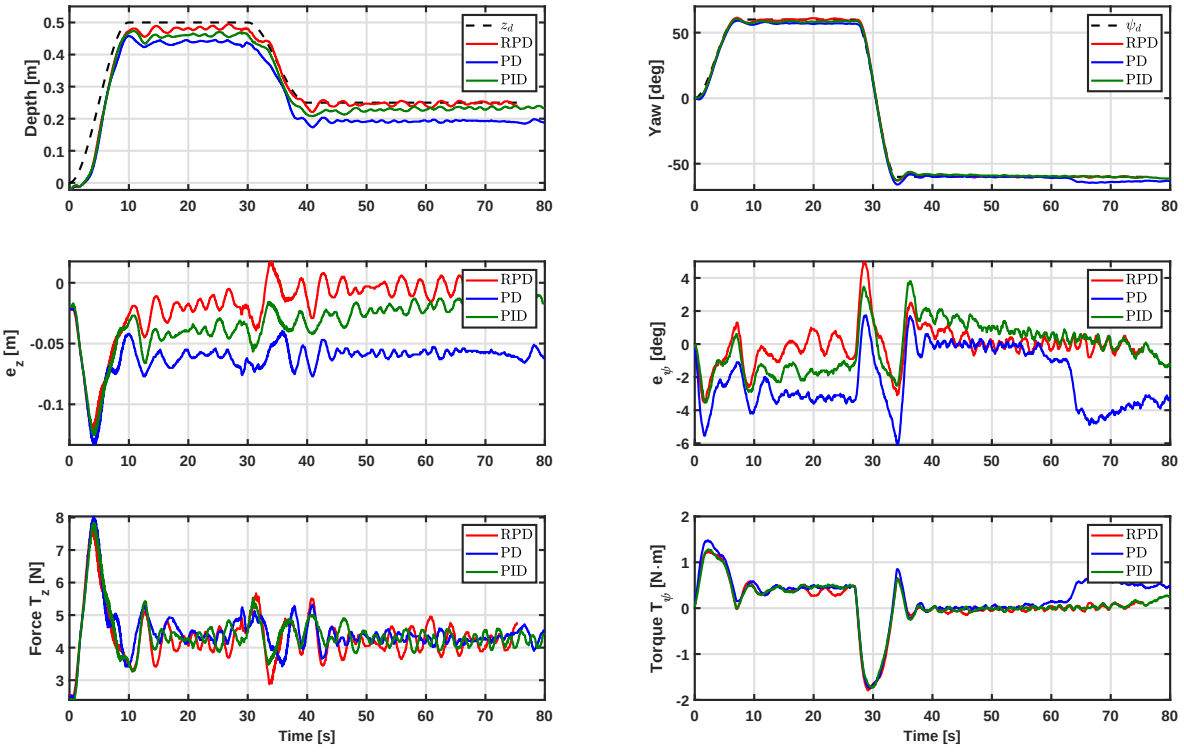


**Figure 7:** Scenario 2- Robustness towards parametric uncertainties. Experimental results of the trajectory tracking in depth and yaw, the desired trajectory is represented by the black dashed line, the PD with a solid blue line, the PID with a solid green line, and the proposed RPD controller with a solid red line.

same disturbance for different controllers. Also, the energy consumption for this scenario is summarized in the fourth row of Table 3.

Finally, the estimated disturbance for the current case is shown in the fourth row of Figure 10.

**Table 2**
RMSE comparison criteria for PD, PID and RPD.

| | PD | | PID | | RPD | |
|---|---|---|---|---|---|---|
| Case | $z$(m) | $\psi$(deg) | $z$(m) | $\psi$(deg) | $z$(m) | $\psi$(deg) |
| 1 | 0.0151 | **0.1418** | 0.0083 | 0.2964 | **0.0027** | 0.2062 |
| 2 | 0.0613 | 2.1718 | 0.0319 | 0.2747 | **0.0173** | **0.0479** |
| 3 | 0.0074 | 1.0053 | **0.0058** | 0.3607 | 0.0068 | **0.1003** |
| 4 | – | – | – | – | **0.0047** | **0.1444** |

## 6.3. Improving non-robust controllers with STA-based disturbance observer

The main objective of the proposed STA-based observer is to estimate external disturbances and parametric uncertainties in finite time. Then, this estimation will be injected into non-robust controllers to improve their trajectory-tracking performance. In previous sections, we observed that the proposed algorithm can enhance the nominal PD controller design. Indeed, we have performed several scenarios to test its robustness against the nominal version and the well-known PID controller. However, the question is to affirm whether or not the proposed disturbance observer is compatible with other control schemes. To answer this question, we will test our proposed disturbance observer with another controller. In this sense, we choose the Backstepping control method. Indeed, the BS is a nonlinear control technique that decomposes a complex nonlinear system into simpler, controllable subsystems. The approach involves designing controllers for each subsystem recursively, progressing *backward* from the system output to the input. Using Lyapunov functions at each step, stability is ensured,

**Table 3**
Energy consumption comparison criteria through the INT indicator for PD, PID and RPD.

| | PD | | PID | | RPD | |
|---|---|---|---|---|---|---|
| Case | Depth | Yaw | Depth | Yaw | Depth | Yaw |
| 1 | 3221 | 414 | 2977 | 388 | 3570 | 323 |
| 2 | 7634 | 731 | 7605 | 540 | 6545 | 479 |
| 3 | 1902 | 509 | 2103 | 567 | 2338 | 573 |
| 4 | – | – | – | – | 3711 | 558 |

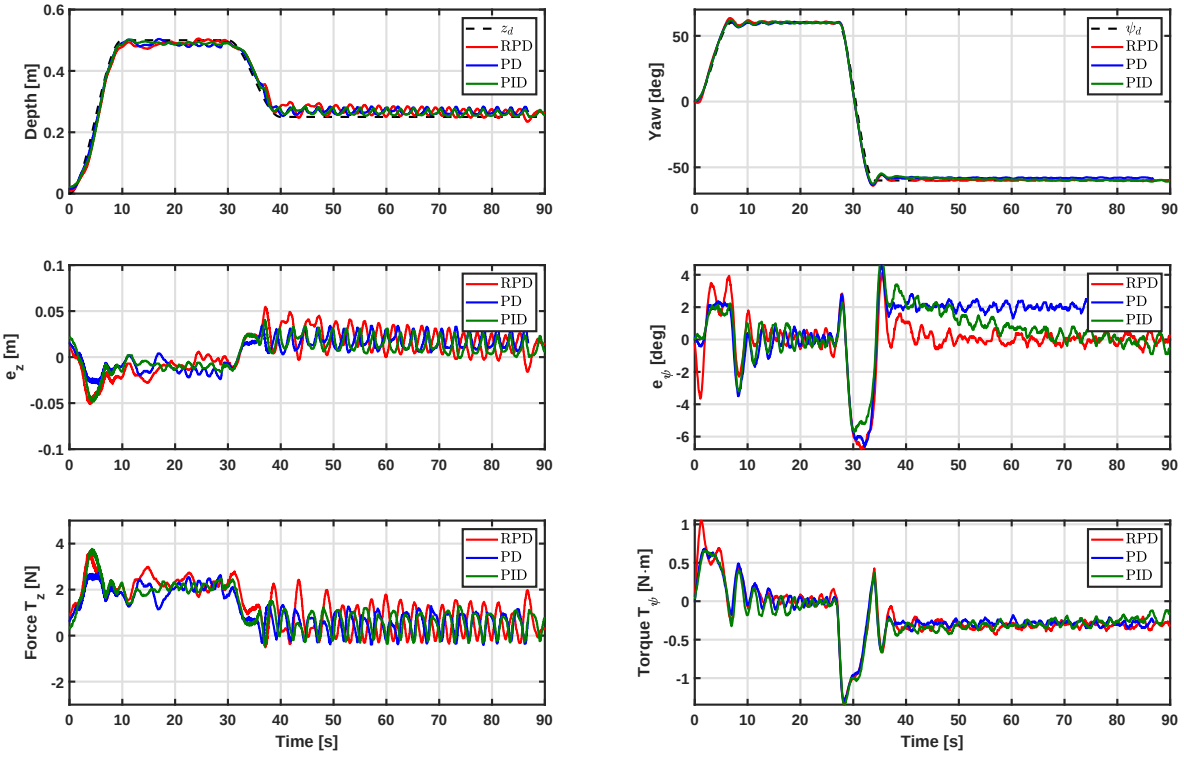


**Figure 8:** Scenario 3- Robustness towards sudden mass change. Experimental results of the trajectory tracking in depth and yaw, the desired trajectory is represented by the black dashed line, the PD with a solid blue line, the PID with a solid green line, and the proposed RPD controller with a solid red line.

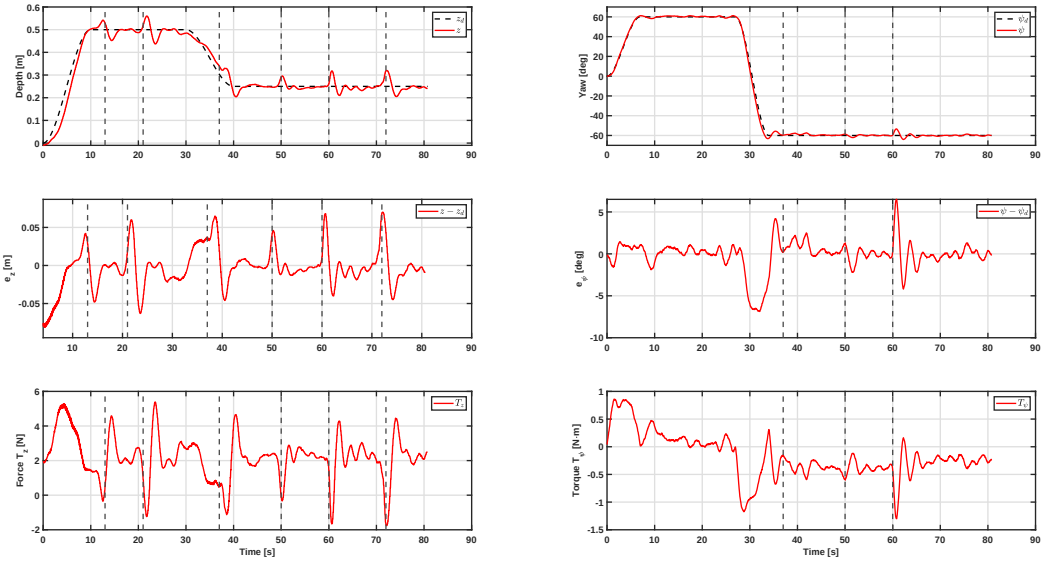


**Figure 9:** Scenario 4- Robustness towards external disturbance rejection. Experimental results of the trajectory tracking in depth and yaw, the desired trajectory is represented by the black dashed line, the PD with solid blue line and the proposed RPD controller with a solid red line.

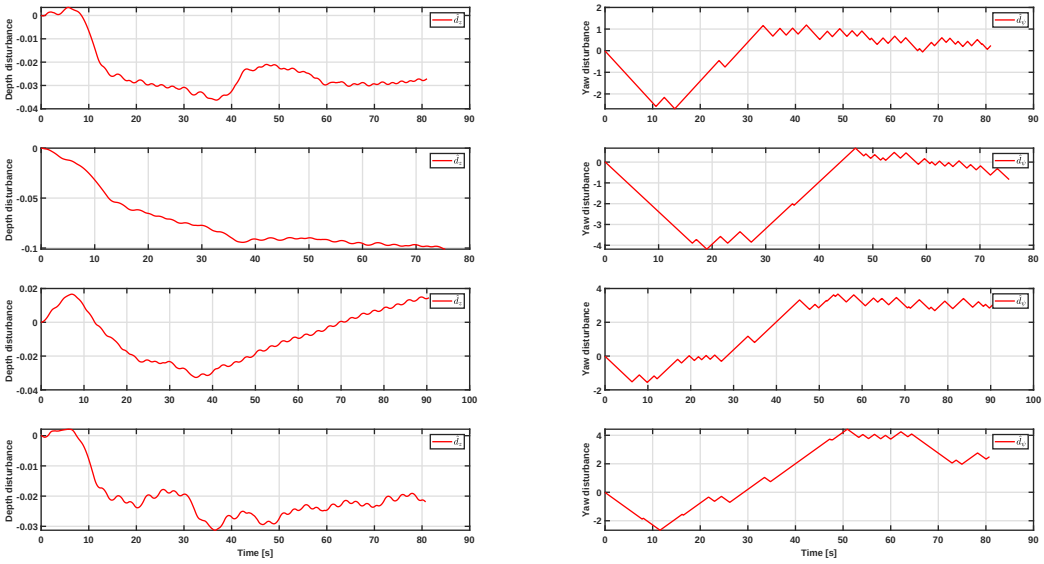


**Figure 10:** Estimated disturbances for depth (left) and yaw (right) dynamics made by the proposed observer. The results for the nominal case, robustness towards parametric uncertainties, robustness towards sudden mass change and robustness towards external disturbances, are shown in the first, second, third and fourth rows of the figure, respectively.

and the global stability of the entire system is achieved by combining Lyapunov functions from all subsystems. This method is particularly effective for managing the control of complex nonlinear systems by addressing each subsystem individually and then integrating the results to attain a global controller ensuring the whole system's stability. In our previous work Guerrero, Torres, Antonio and Campos (2018), we have developed a BS controller which has the following structure:

$$\tau_\eta = \hat{G}(z)\Big[\ddot{z}_1^d - e_1 - \hat{F}(z) + \Gamma(\Gamma e_1 - e_2) - \Upsilon e_2\Big] \quad (38)$$

where $\ddot{z}_1^d$ is the second time derivative of the desired trajectory. The tracking errors are represented by $e_1 = z_1 - z_1^d$ and $e_2 = \dot{e}_1 + \Gamma e_1$, and the matrices $\Gamma = \text{diag}\{\gamma_1, \cdots, \gamma_6\}$ and $\Upsilon = \text{diag}\{\upsilon_1, \cdots, \upsilon_6\}$ are selected diagonal and positive definite.

The proposed controller (38) was validated on the underwater robot *LIRMIA III* and from the trajectory tracking results we observed that the BS shows a small constant steady-state error during those experiments. Then, motivated by this drawback, we test also this controller on *Leonard* underwater vehicle. Also, we propose to compare its performance against the robust Backstepping (RBS) which yields from the combination of the nominal BS controller given by (38), and the proposed STA-disturbance observer (13). The control law of the resulting RBS is defined as follows:

$$\tau_\eta = \hat{G}(z)\Big[\ddot{z}_1^d - e_1 - \hat{F}(z) + \Gamma(\Gamma e_1 - e_2) - \Upsilon e_2 - \hat{d} - \hat{K}\,\text{SGN}(e_2)\Big] \quad (39)$$

Here, the $\hat{d}$ is the estimated external disturbance provided by the observer. The vector $\text{SGN}(e_2) \in \mathbb{R}^6$ and $\hat{K}$ is a dynamic adaptive gain, computed as follows:

$$\dot{\hat{K}} = \beta_{BS}\|e_2\| \quad (40)$$

where $\beta_{BS} \in \mathbb{R}$ is a positive constant.

Due to lack of space, we have compared the trajectory tracking performance of the control laws (38) and (39) under Scenario 1 (nominal case) and Scenario 2 (robustness towards parametric uncertainties), only.

In Figure 11 we plot the results of trajectory tracking under the nominal scenario. In the left upper part of the figure, we can observe the performance of the BS (solid blue line) and the RBS (solid red line) when they are tracking a trajectory (dashed black line). One can observe that both controllers show a good tracking performance. Also, in the right upper part of the figure, we have plotted the yaw trajectory tracking, and we can notice also the good tracking performance of both controllers. In the middle of the figure, we show the corresponding trajectory tracking errors for both experiments. It is important to highlight that the introduction of the disturbance observer improves the tracking performance of both dynamics depth and yaw. Finally, at the bottom of the figure, we plot the evolution versus time of the control inputs. As we can see, both controllers spend almost the same amount of energy.

The obtained results for the trajectory tracking under parametric uncertainties are displayed in Figure 12. In the left upper part of the figure, we can observe the performance of the proposed controllers for the depth trajectory task. As we can observe, the RBS outperforms the BS, showing a lower tracking error, as can also be confirmed by the plot of the middle part of the figure. Besides, the RBS shows an improvement w.r.t the BS for the yaw trajectory tracking.

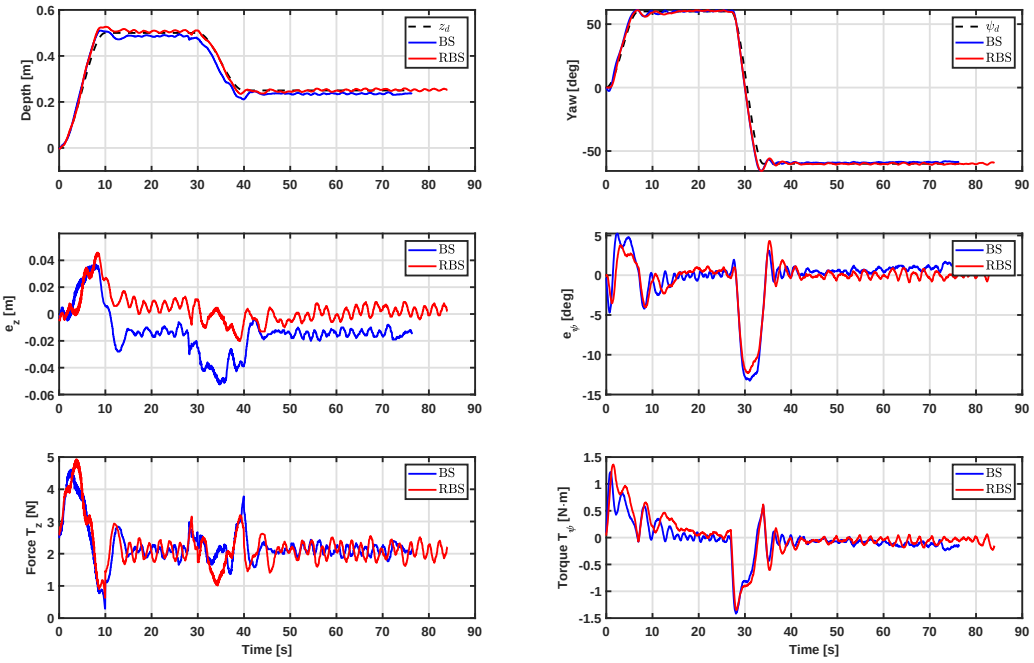


**Figure 11:** Scenario 1- Nominal Case. Experimental results of the trajectory tracking in depth and yaw, the desired trajectory is represented by the black dashed line, the BS with a solid blue line, and the proposed RBS controller with a solid red line.

In addition, at the bottom of the figure, the evolution of the control input signals is depicted for both controllers. Finally, the better performance of the RBS over the BS is numerically confirmed by the RMSE summarized in Table 4.

**Table 4**
RMSE comparison criteria for BS and RBS.

| | PD | | RBS | |
|---|---|---|---|---|
| Case | $z$(m) | $\psi$(deg) | $z$(m) | $\psi$(deg) |
| 1 | 0.0136 | **0.3422** | **0.0034** | 0.5486 |
| 2 | 0.0565 | 1.1641 | **0.0018** | **0.4423** |

## 7. Conclusions and Future work

The present contribution deals with robustifying the famous and widely used classical PD controller when applied to the trajectory tracking problem in AUVs. For this purpose, a disturbance observer based on STA is proposed, which has properties of convergence in finite time, reduced chattering, and is robust to matching disturbances. In the theoretical part, the Lyapunov stability analysis of the closed-loop controller-observer scheme is presented. The experimental investigation consists of a comprehensive real-time study to test the capacities of the proposed scheme, including undisturbed cases, parametric disturbances, and external disturbances. In summary, the proposed control scheme, consisting of a PD controller assisted by an STA-based disturbance observer, presents essential advantages over PD controller alone, both in performance and robustness against parametric and external disturbances. At the same time, the proposed design preserves the simplicity of the PD controller as only two parameters of the STA observer are required to be adjusted. The future work will consist in analyzing and synthesizing the adaptive version of the proposed disturbance observer and its real-time experimental validation.

## Acknowledgements

The French Occitanie Region supported this work within the project "Défi-clé Robotique Centrée sur l'Humain" under Grant N° 21034741.

## A. Description of the UUV dynamic model

The matrices of the body-fixed frame dynamic model (1) are detailed in the sequel.
The inertia matrix is defined as $M = M_{RB} + M_A$, where:

$$M_{RB} = \begin{bmatrix} m & 0 & 0 & 0 & mz_G & -my_G \\ 0 & m & 0 & -mz_G & 0 & mx_G \\ 0 & 0 & m & my_G & -mx_G & 0 \\ 0 & -mz_G & my_G & I_x & -I_{xy} & -I_{zx} \\ mz_G & 0 & -mx_G & -I_{yx} & I_y & -I_{yz} \\ -my_G & mx_G & 0 & -I_{zx} & -I_{zy} & I_z \end{bmatrix} \tag{41}$$

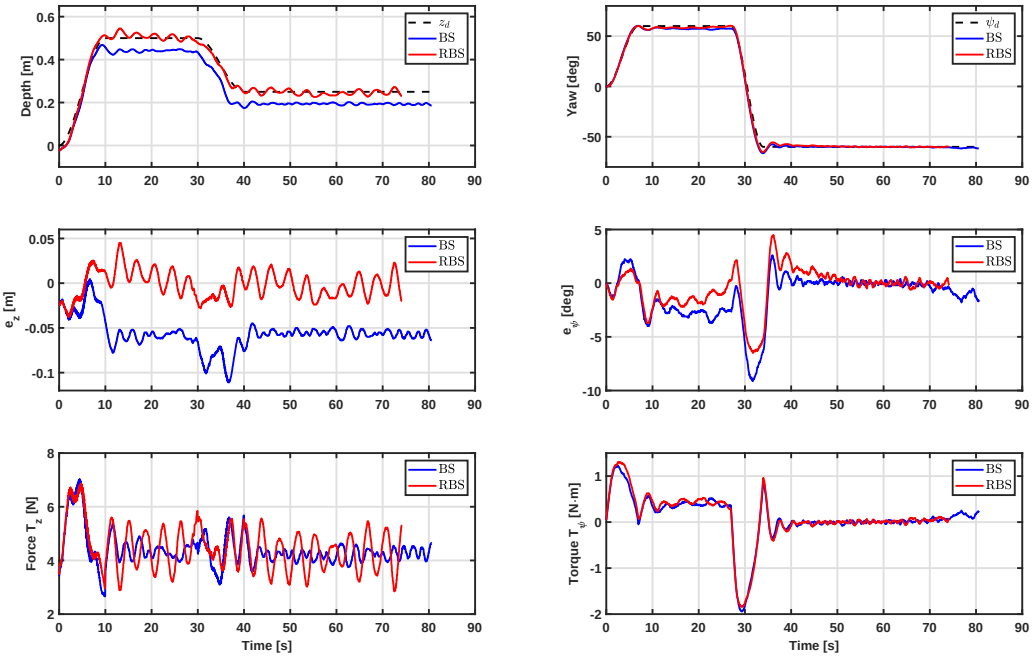


**Figure 12:** Scenario 2- Robustness towards parametric uncertainties. Experimental results of the trajectory tracking in depth and yaw, the desired trajectory is represented by the black dashed line, the BS with a solid blue line, and the proposed RBS controller with a solid red line.

$$M_A = -\begin{bmatrix} X_{\dot{u}} & X_{\dot{v}} & X_{\dot{w}} & X_{\dot{p}} & X_{\dot{q}} & X_{\dot{r}} \\ Y_{\dot{u}} & Y_{\dot{v}} & Y_{\dot{w}} & Y_{\dot{p}} & Y_{\dot{q}} & Y_{\dot{r}} \\ Z_{\dot{u}} & Z_{\dot{v}} & Z_{\dot{w}} & Z_{\dot{p}} & Z_{\dot{q}} & Z_{\dot{r}} \\ K_{\dot{u}} & K_{\dot{v}} & K_{\dot{w}} & K_{\dot{p}} & K_{\dot{q}} & K_{\dot{r}} \\ M_{\dot{u}} & M_{\dot{v}} & M_{\dot{w}} & M_{\dot{p}} & M_{\dot{q}} & M_{\dot{r}} \\ N_{\dot{u}} & N_{\dot{v}} & N_{\dot{w}} & N_{\dot{p}} & N_{\dot{q}} & N_{\dot{r}} \end{bmatrix} \tag{42}$$

with $m$ the mass of the vehicle, $I_x$, $I_y$ and $I_z$ are the moments of inertia about the $X_0$, $Y_0$ and $Z_0$-axes and $I_{xy} = I_{yx}$, $I_{xz} = I_{zx}$, and $I_{yz} = I_{zy}$ are the products of inertia. The position of the center of gravity is defined by $x_G$,$y_G$ and $z_G$. The elements of the added inertia matrix, $M_A$, are defined in Fossen (1999).

The Coriolis matrix is defined as $C(\nu) = C_A(\nu) + C_{RB}(\nu)$, where:

$$C_A(\nu) = \begin{bmatrix} C_{A_{11}} & C_{A_{12}} \\ C_{A_{21}} & C_{A_{22}} \end{bmatrix} \tag{43}$$

where $C_{A_{11}} = 0_{3\times3}$, and $C_{A_{21}} = -C_{A_{12}}^T$, with:

$$C_{A_{12}} = \begin{bmatrix} 0 & -Z_{\dot{w}}w & Y_{\dot{v}}v \\ Z_{\dot{w}}w & 0 & -X_{\dot{u}}u \\ -Y_{\dot{v}}v & X_{\dot{u}}u & 0 \end{bmatrix}$$

$$C_{A_{22}} = \begin{bmatrix} 0 & -N_{\dot{r}}r & M_{\dot{q}}q \\ N_{\dot{r}}r & 0 & -K_{\dot{p}}p \\ -M_{\dot{q}}q & K_{\dot{p}}p & 0 \end{bmatrix}$$

$$C_{RB}(\nu) = \begin{bmatrix} C_{11} & C_{12} \\ C_{21} & C_{22} \end{bmatrix} \tag{44}$$

where $C_{11} = 0_{3\times3}$

$$C_{12} = \begin{bmatrix} m(y_Gq + z_Gr) & -m(x_Gq - w) & -m(x_Gr + v) \\ -m(y_Gp + w) & m(z_Gr + x_Gp) & -m(y_Gr - u) \\ -m(z_Gp - v) & -m(z_Gq + u) & m(x_Gp + y_Gq) \end{bmatrix}$$

and $C_{21} = -C_{12}^T$, and

$$C_{22} = \begin{bmatrix} 0 & \star & \star\star \\ -\star & 0 & \star\star\star \\ -\star\star & -\star\star\star & 0 \end{bmatrix}$$

where:

$$\star = -I_{yz}q - I_{xz}p + I_zr \tag{45}$$

$$\star\star = I_{yz}r + I_{xy}p - I_yq \tag{46}$$

$$\star\star\star = -I_{xz}r - I_{xy}q + I_xp \tag{47}$$

Finally, it is worth noting that $C(\nu)$ is skew-symmetrical. The damping matrix, $D(\nu)$, is defined as:

$$D(\nu) = -\text{diag}\{X_u, Y_v, Z_w, K_p, M_q, N_r\}$$
$$-\text{diag}\{X_{u|u|}|u|, Y_{v|v|}|v|, Z_{w|w|}|w|, K_{p|p|}|p|, M_{q|q|}|q|, N_{r|r|}|r|\}$$

where $\{X_u, Y_v, Z_w, K_p, M_q, N_r\}$ are the linear damping hydrodynamic terms, and $\{X_{u|u|}, Y_{v|v|}, Z_{w|w|}, K_{p|p|}, M_{q|q|}, N_{r|r|}\}$

are the quadratic damping hydrodynamic elements.
The gravity vector, $g(\eta)$, is defined as follows:

$$g(\eta) = \begin{bmatrix} W_B s\theta \\ -W_B c\theta s\phi \\ -W_B c\theta c\phi \\ -(y_G W - y_B B)c\theta c\phi + (z_G W - z_B B)c\theta s\phi \\ (z_G W - z_B B)s\theta + (x_G W - x_B B)c\theta c\phi \\ -(x_G W - x_B B)c\theta s\phi + (y_G W - y_B B)s\theta \end{bmatrix} \tag{48}$$

where $W_B = W - B$, with $W$ and $B$ representing the weight and the buoyancy of the vehicle.
The transformation matrix, $J(\eta)$, given in (2) is explicitly defined as follows:

$$J(\eta) = \begin{bmatrix} J_1(\eta) & 0_{3\times3} \\ 0_{3\times3} & J_2(\eta) \end{bmatrix} \tag{49}$$

where

$$J_1(\eta) = \begin{bmatrix} c\psi c\theta & -s\psi c\phi + c\psi s\theta s\phi & s\psi s\phi + c\psi c\phi s\theta \\ s\psi c\theta & c\psi c\phi + s\psi s\theta s\phi & -c\psi s\phi + s\psi s\phi s\theta \\ -s\theta & c\theta s\phi & c\theta c\phi \end{bmatrix}$$

and

$$J_2(\eta) = \begin{bmatrix} 1 & s\phi t\theta & c\phi t\theta \\ 0 & c\phi & -s\phi \\ 0 & s\phi/c\theta & c\phi/c\theta \end{bmatrix}$$

Where, for simplicity, we adopted the shorthand notations $\cos(\star) = c\star$, $\sin(\star) = s\star$ and $\tan(\star) = t\star$.
Finally, the matrices of the dynamic model with respect to the earth-fixed frame shown in (3) can be obtained using the relations developed in (4). However, the computation of these matrices may produce very complex mathematical expressions for each matrix element. Moreover, the full and exact knowledge of the hydrodynamic parameters is very complicated because they may vary depending on the operating conditions. To simplify the computation of the estimated matrices, based on the symmetry of the vehicle and assuming that it is moving at low speeds. Then, based on Fossen (1999), we can reduce the number of parameters of each matrix and they can be found following the experimental approach given in Campos et al. (2017). For the case of *Leonard* vehicle, we computed the following representation for the inertia matrix:

$$\begin{aligned} \hat{M} =& \text{diag}\{m, m, m, I_x, I_y, I_z\} \\ =& \text{diag}\{28, 28, 28, 0.35, 0.69, 0.65\} \end{aligned} \tag{50}$$

The damping matrix is given as follows:

$$\hat{D}_\eta = \begin{bmatrix} 30 + 40s^2\psi & -20s(2\psi) & 0 & 0 & 0 & 0 \\ -20s(2\psi) & 70 - 40s^2\psi & 0 & 0 & 0 & 0 \\ 0 & 0 & 80 & 0 & 0 & 0 \\ 0 & 0 & 0 & 1.4 & 0 & 0 \\ 0 & 0 & 0 & 0 & 2.5 & 0 \\ 0 & 0 & 0 & 0 & 0 & 2.9 \end{bmatrix} \tag{51}$$

Here, it is worth noting that the damping matrix $\hat{D}_\eta$ is positive definite.
The gravity vector is defined as follows:

$$\hat{g}(\eta) = \begin{bmatrix} W_B s\theta \\ -W_B c\theta s\phi \\ -W_B c\theta c\phi \\ -z_B B c\theta s\phi \\ z_B B s\theta \\ 0 \end{bmatrix} \tag{52}$$

Finally, considering that the $\theta$ and $\phi$ of the vehicle are stable by design, we can simplify the construction of the transformation matrix as follows:

$$J(\eta) = \begin{bmatrix} J_{1,1}(\psi) & 0_{3\times3} \\ 0_{3\times3} & I_{3\times3} \end{bmatrix} \tag{53}$$

with $J_{1,1}(\psi) = \begin{bmatrix} c\psi & -s\psi & 0 \\ s\psi & c\psi & 0 \\ 0 & 0 & 1 \end{bmatrix}$.

## CRediT authorship contribution statement

**Jesus Guerrero:** Conceptualization of this study, Methodology, Software, Data collection, Original draft preparation. **Ahmed Chemori:** Software, Writing, Data Collection - Original draft preparation. **Vincent Creuze:** Software, Writing - Original draft preparation. **Jorge Torres:** Writing, Original and final draft preparation.

## References


An, S., Wang, L., He, Y., Yuan, J., 2022. Adaptive backstepping sliding mode tracking control for autonomous underwater vehicles with input quantization. Advanced Theory and Simulations 5, 2100445.

Bessa, W.M., Dutra, M.S., Kreuzer, E., 2008. Depth control of remotely operated underwater vehicles using an adaptive fuzzy sliding mode controller. Robotics and Autonomous Systems 56, 670–677.

Bessa, W.M., Dutra, M.S., Kreuzer, E., 2010. An adaptive fuzzy sliding mode controller for remotely operated underwater vehicles. Robotics and Autonomous Systems 58, 16–26.

Boyd, S., El Ghaoui, L., Feron, E., Balakrishnan, V., 1994. Linear matrix inequalities in system and control theory. SIAM.

Campos, E., Chemori, A., Creuze, V., Torres, J., Lozano, R., 2017. Saturation based nonlinear depth and yaw control of underwater vehicles with stability analysis and real-time experiments. Mechatronics 45, 49–59.

Campos, E. Monroy, J., Abundis, H., Chemori, A., Creuze, V., Torres, J., 2019. A nonlinear controller based on saturation functions with variable parameters to stabilize an AUV. International Journal of Naval Architecture and Ocean Engineering 11, 211–224. doi:https://doi.org/10.1016/j.ijnaoe.2018.04.002.

Chen, W.H., 2003. Nonlinear disturbance observer-enhanced dynamic inversion control of missiles. Journal of Guidance, Control, and Dynamics 26, 161–166.

Cui, R., Yang, C., Li, Y., Sharma, S., 2017. Adaptive neural network control of auvs with control input nonlinearities using reinforcement learning. IEEE Transactions on Systems, Man, and Cybernetics: Systems 47, 1019–1029.

Elmokadem, T., Zribi, M., Youcef-Toumi, K., 2016. Trajectory tracking sliding mode control of underactuated auvs. Nonlinear Dynamics 84, 1079–1091.

Fossen, T.I., 1999. Guidance and control of ocean vehicles. University of Trondheim, Norway, Printed by John Wiley & Sons, Chichester, England, ISBN: 0 471 94113 1, Doctors Thesis .

Ginoya, D., Shendge, P., Phadke, S., 2013. Sliding mode control for mismatched uncertain systems using an extended disturbance observer. IEEE Transactions on Industrial Electronics 61, 1983–1992.

Guerrero, J., Chemori, A., Torres, J., Creuze, V., 2023. Time-delay high-order sliding mode control for trajectory tracking of autonomous underwater vehicles under disturbances. Ocean Engineering 268, 113375. doi:https://doi.org/10.1016/j.oceaneng.2022.113375.

Guerrero, J., Chemori, A., Torres, J., Creuze, V., 2024. Sta-based design of an adaptive disturbance observer for autonomous underwater vehicles: From concept to real-time validation. Control Engineering Practice 144, 105831.

Guerrero, J., Torres, J., Antonio, E., Campos, E., 2018. Autonomous underwater vehicle robust path tracking: Generalized super-twisting algorithm and block backstepping controllers. Journal of Control Engineering and Applied Informatics 20, 51–63.

Guerrero, J., Torres, J., Creuze, V., Chemori, A., 2019a. Observation-based nonlinear proportional–derivative control for robust trajectory tracking for autonomous underwater vehicles. IEEE journal of oceanic engineering 45, 1190–1202.

Guerrero, J., Torres, J., Creuze, V., Chemori, A., 2019b. Trajectory tracking for autonomous underwater vehicle: An adaptive approach. Ocean Engineering 172, 511–522.

Guerrero, J., Torres, J., Creuze, V., Chemori, A., Campos, E., 2019c. Saturation based nonlinear pid control for underwater vehicles: Design, stability analysis and experiments. Mechatronics 61, 96–105.

Han, J., 1995. A class of extended state observers for uncertain systems. Control and decision 10, 85–88.

Han, J., 2009. From pid to active disturbance rejection control. IEEE transactions on Industrial Electronics 56, 900–906.

Herman, P., 2009. Decoupled pd set-point controller for underwater vehicles. Ocean Engineering 36, 529–534.

Li, S., Yang, J., Chen, W.H., Chen, X., 2011. Generalized extended state observer based control for systems with mismatched uncertainties. IEEE Transactions on Industrial Electronics 59, 4792–4802.

Maalouf, D., Creuze, V., Chemori, A., 2012. A novel application of multivariable l1 adaptive control: From design to real-time implementation on an underwater vehicle, in: "Proc. IEEE/RSJ Int. Conf. Intel. Robots and Systems., Algarve, Portugal.

Moreno, J.A., 2009. A linear framework for the robust stability analysis of a generalized super-twisting algorithm, in: 2009 6th International Conference on Electrical Engineering, Computing Science and Automatic Control (CCE), IEEE. pp. 1–6.

Moreno, J.A., Osorio, M., 2008. A lyapunov approach to second-order sliding mode controllers and observers, in: 2008 47th IEEE conference on decision and control, IEEE. pp. 2856–2861.

Nerkar, S., Londhe, P., Patre, B., 2022. Design of super twisting disturbance observer based control for autonomous underwater vehicle. International Journal of Dynamics and Control 10, 306–322.

Orlov, Y., 2004. Finite time stability and robust control synthesis of uncertain switched systems. SIAM Journal on Control and Optimization 43, 1253–1271.

Qiao, L., Zhang, W., 2019. Trajectory tracking control of auvs via adaptive fast nonsingular integral terminal sliding mode control. IEEE Transactions on Industrial Informatics 16, 1248–1258.

Remmas, W., Chemori, A., Kruusmaa, M., 2021. Diver tracking in open waters: A low-cost approach based on visual and acoustic sensor fusion. Journal of Field Robotics 38, 494–508. doi:https://doi.org/10.1002/rob.21999.

Sarhadi, P., Noei, A.R., Khosravi, A., 2016. Model reference adaptive pid control with anti-windup compensator for an autonomous underwater vehicle. Robotics and Autonomous Systems 83, 87–93.

Tijjani, A.S., Chemori, A., Ali, S.A., Creuze, V., 2023. ContinuousâĂŞdiscrete observation-based robust tracking control of underwater vehicles: Design, stability analysis, and experiments. IEEE Transactions on Control Systems Technology 31, 1477–1492. doi:10.1109/TCST.2022.3224321.

Tijjani, A.S., Chemori, A., Creuze, V., 2021. Robust adaptive tracking control of underwater vehicles: Design, stability analysis and experiments. IEEE/ASME Transactions on Mechatronics 26, 897–907. doi:10.1109/TMECH.2020.3012502.

Tijjani, A.S., Chemori, A., Creuze, V., 2022. A survey on tracking control of unmanned underwater vehicles: Experiments-based approach. Annual Reviews in Control 54, 125–147.

Wadoo, S., Kachroo, P., 2017. Autonomous underwater vehicles: modeling, control design and simulation. CRC press.

Wang, B., Meng, Z., Huang, P., 2017. Attitude control of towed space debris using only tether. Acta Astronautica 138, 152–167.

Wang, B., Mihalec, M., Gong, Y., Pompili, D., Yi, J., 2018. Disturbance observer-based motion control of small autonomous underwater vehicles, in: Dynamic Systems and Control Conference, American Society of Mechanical Engineers. p. V003T35A004.

Xiang, X., Yu, C., Zhang, Q., 2017. Robust fuzzy 3d path following for autonomous underwater vehicle subject to uncertainties. Computers & Operations Research 84, 165–177.

**Jesus GUERRERO** received a Ph.D. degree in automatic control from the Center for Research and Advanced Studies of the National Polytechnic Institute (CINVESTAV), Mexico City, Mexico, in 2019. He is currently an associate professor at TecnolÃşgico Nacional de MÃŕxico/ITS Abasolo. His research interests include nonlinear, adaptive, and time-delay control and their applications in underactuated systems, ground, aerial, and underwater vehicles.

**Ahmed CHEMORI** received the M.Sc. and Ph.D. degrees both in automatic control from the Grenoble Institute of Technology, Grenoble, France, in 2001 and 2005, respectively. He has been a Postdoctoral Fellow with the Automatic Control Laboratory, Grenoble, France, in 2006. He is currently a senior CNRS Researcher in automatic control and robotics with the Montpellier Laboratory of Informatics, Robotics and Microelectronics (LIRMM-CNRS). His research interests include nonlinear robust, adaptive, and predictive control and their real-time applications in complex robotic systems including (i) underwater robots, (ii) parallel robots, (iii) wearable robots, and (iv) underactuated robots.

**Vincent CREUZE** received his Ph.D. degree in 2002 from the University Montpellier 2 (France). He is currently a full Professor at the University of Montpellier, attached to the Robotics Department of LIRMM. His research interests include design, modeling, sensing, and control applied to underwater robots for deep archaeological applications or marine biology.

**Jorge TORRES** received his Ph.D. degree in Automatic Control from the National Polytechnique Institute-Grenbole, France, in 1990. He joined the Department of Electrical Engineering at the CINVESTAV, Mexico, in 1990. Dr. Torres spent a sabbatical year at the Institute of Research in Communications and Cybernetics, IRCCYN-Nantes, France, from 1997-1998. His research interest lies in the structural approach of linear systems, stability of multivariate polynomials, and applied nonlinear control to mini-uuv and bioprocess control.